Original Research Paper

IJES *Iranian Journal of Earth Sciences*
Vol. 14, No. 3, 2022, 221-240.
DOI: 10.30495/IJES.2021.685396

Facies analysis, sedimentation conditions and geochemistry of clastic deposits of Ashin formation (Late Ladinian-Early Carnian), Northeast of Nain, East of Central Iran

Payman Rezaee*[1], Mohammad Khanehbad[2], Moasoumeh Ezatifar[1], Seyedeh Akram Jooybari[1], Kiamars Hosseini[1]

1. Department of Geology, University of Hormozgan, Bandar Abbas, Iran
2. Department of Geology, Faculty of Science, Ferdowsi University of Mashhad, Mashhad, Iran

Received 25 April 2020; accepted 23 July 2020

Abstract
The present study aims to investigate the petrographic, geochemical features, and depositional facies of the Late Triassic Ashin Formation (Nakhlak Group, central Iran). For this purpose, 100 thin sections, and 13 samples of fine-grained sedimentary rocks were analyzed for their petrographic and geochemical characteristics, taken from a 330-m thick section of this formation. The petrographic types identified in this formation include sandstone, siltstone and limestone. This study suggests limestone facies are deposited in upper parts of the distal submarine fan towards the shore, sandstone facies are deposited in the middle part of the distal submarine fan, and the shale facies are deposited in lower parts of the distal submarine fan towards the abyssal plain by turbidity currents. The plotting of petrographic data on ternary diagrams for compositional classification illustrate their composition as litharenites, sub-litharenites, and a few litharenite-feldspathic and shales. Discrete diagrams refer to a tectonic setting of a continental arc complex and the active continental margin. The results of the modal analysis and geochemical data indicate the orogenic re-cycling for these deposits. CIA and CIW indexes indicate moderate weathering of the source area under semi-arid to semi-humid climates.
Keywords: *Facies Analysis, Provenance, Geochemistry, Ashin Formation.*

1. Introduction
Full understanding of clastic sequences requires geometrical and lateral relevance of sequences, lithological changes, and facies studies (Flugel 2010). In addition, the detection of facies sets can contribute to the reconstruction of the sedimentary environment and depositional conditions (Catuneanu 2006; Miall 2000). The Triassic sedimentary successions in northwestern Anarak in central Iran are restricted and distinct from other coeval sequences in the Nakhlak region, which resemble the Darband group in northeastern Iran (Davoudzadeh abd Seyed-Emami 1972; Alavi et al. 1997; Vaziri 2011). These sequences are very similar to the sequence of sediments in northern Afghanistan and deposited in an epi-continental sea (Ghorbani 2019). The provenance study involves the interpretation of the source of lithology of siliciclastic sedimentary clastic rocks (Nagarajan et al. 2017). Siliciclastic deposits are always impacted by factors such as source rock type, weathering, transportation distance, and diagenetic changes after deposition (Von Eynatten 2003; Jin et al. 2006; Gabo et al. 2009; Nagarajan et al. 2017; Nikbakht et al. 2019).

The provenance study of sedimentary rocks is possible based on their geochemical and mineralogical composition. A large number of researchers have investigated the relationship between the tectonic setting, origin and composition of siliciclastic deposits (e.g., Dickinson and Suczek 1979; Bhatia and Crook 1986; Cullers 1994; Armstrong-Altrin et al. 2004; Jafarzadeh and Hosseini-Barzi 2008, Azizi et al. 2018b; Azizi 2018). The geochemistry of the major, trace and rare earth elements of siliciclastic sediments provides some information on the types of source rocks and tectonic setting of the sedimentary basins (Nesbitt and Young 1982; Cullers 1995; Armstrong-Altrin et al. 2004; Nagarajan et al. 2014; Armstrong-Altrin et al. 2015). The geochemical characteristics of tectonic-magmatic events in sedimentary rocks are well-preserved (Raza et al. 2010) and are considered an important tool for studying the evolution of the Earth's crust (Jahn et al. 1981; Taylor and Mclennan 1985; Condie 1993). Geochemical studies in clastic rocks complement petrographic studies, especially when geological processes have altered primary mineralogy (Cullers 1994 and 1995). Although diagenesis and subsurface leaching cause some problems in interpreting provenance (McBride 1985; Blatt 1985), sandstone geochemistry is considered a powerful tool in determining the provenance (Zimmermann and Bahlburg 2003). In addition, the source composition is preserved and provenance determination in shales is important due to their very fine grain size and permeability (Hessler and Lowe 2006; Azizi and Rezaee 2014; Zaid and Al-Gahtani 2015; Ali et al. 2017; Azizi et al. 2018a; 2018b). In this study, petrographic sedimentary and geochemical data were used in order to evaluate the provenance, tectonic setting and palaegeography of the Ashin Formation (late Ladinian-Early Carnian). The results of this study can

*Corresponding author.
E-mail address (es): p.rezaee@hormozgan.ac.ir

help to better understand the sedimentary conditions of late Ladinian-Early Carnian deposits in other sedimentary-structural areas of Iran and the world.

2. Geological setting

The study area is located in central Iran (60 km northeast of Anarak) and constitutes part of the Nakhlak Group on the Central Iran Plate, (Fig 1). The Nakhlak Group is one of the most controversial stratigraphic and tectonic units on the Iranian plate (Davuodzadeh and Seyed-Emami1972; Ruttner 1991 and 1993; Seyed-Emami 2003; Balini et al. 2009).

This group consists of three stratigraphic formations from base to top: the Elm, Baqrogh, and Ashin formations (e.g., Davoudzadeh and Syed-Emami 1972; Alavi et al. 1997; Vaziri 2001; Balini et al. 2009). The Ashin Formation, the youngest of the Nakhlak Group, includes interbedded sandstone and shale (Vaziri, 2001;Hashemi Azizi et al. 2017; Azizi et al, 2018b). The Ashin Formation's main outcrop exposures are located along the 40′ 53˚ eastern latitude and 34′ 33˚ northern latitude. The Ashin Formation in the studied section overlies the Baqoroq Formation with an erosional unconformity/contact and underlies late Cretaceous deposits with a tectonic contact. A view of the lower and upper boundaries of the Ashin Formation is illustrated in Fig 2.

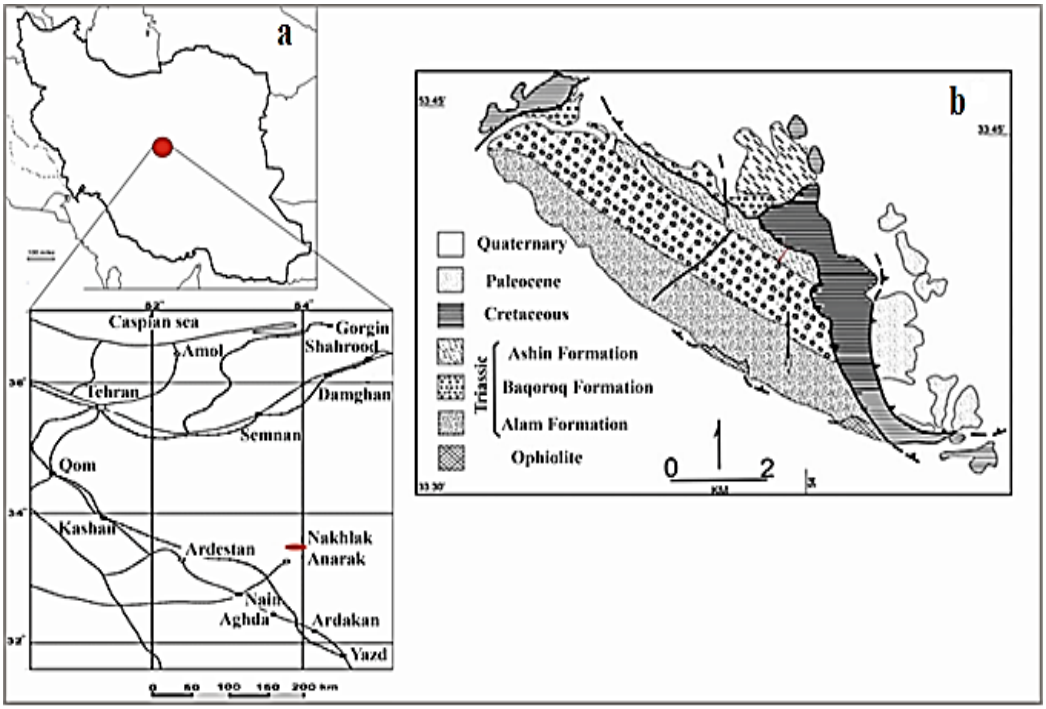

Fig 1. a) Geographical location of Nakhlak area on the map of Iran (Red Square: Nakhlak area) and roadmap of access to the study area (Iran Roads Atlas). b) geological map of the Nakhlakh Group and the Ashin Formation of this group (red double arrow: study section) (Alavi et al. 1997)

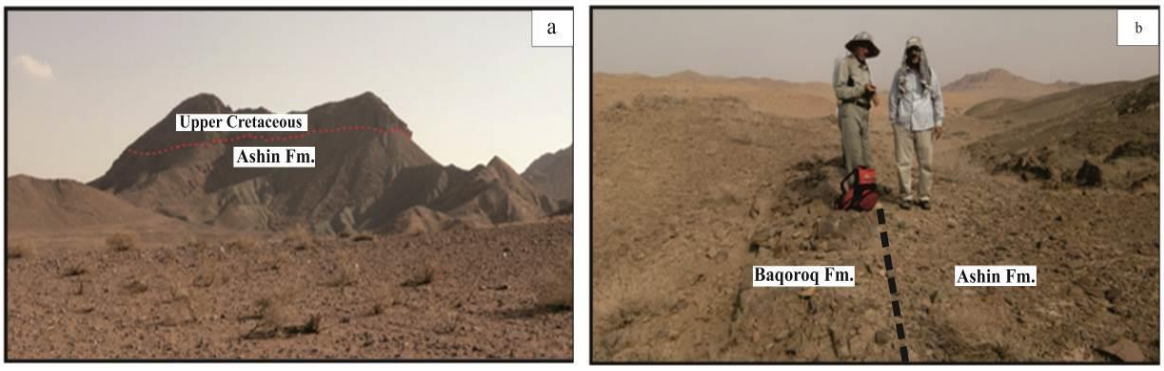

Fig 2. a) View of the upper contact of the Ashin Formation with Late Cretaceous calcareous deposits (looking to the East), and b) View of the lower contact of the Ashin Formation with the Baqoroq Formation (looking at the East).

3. Methodology

In this study, the thickness of sedimentary layers was measured through a tape measure, a compass and a Jacob's rod based on two steps of reciprocal correction (Coe, 2003). Macro scale sedimentary structures, lithofacies, fossil content, and structural complications such as slumping structures were recorded. Then, 100 samples were selected and evaluated based on quantitative and qualitative laboratory studies. Petrographic studies were performed in the laboratory of the Department of Geology at the University of Hormozgan using a BK-230 polarizing microscope. The methods of Folk (1980) and Pettijohn et al. (1987) were used for determining clastic facies. The classification methods presented by Dunham (1962), Embry and Klovan (1971), and their comparison with standard facies classification (Flugel 2010; Wilson 1975) were used for determining carbonate facies. In addition, point-counting of 13 thin sections of sandstones based on the Gazzi-Dickinson method (Ingersoll et al. 1984) was performed and four to five hundred grains were counted in each thin section. In addition, shale samples were analyzed using XRD methodology at the Binaloud Spectrum Minerals Research Company for determining the mineralogy of fine-grained facies. XRF analysis of powdered samples was used for determining major element contents (Rollinson 1993). 13 sandstones with the lowest weathering and calcium carbonate content, as well as 11 shale samples with the lowest calcium carbonate content were selected for XRF geochemical analysis. The data obtained from point-counting and geochemical analysiswere plotted in various classification diagrams and the results are discussed below.

4. Lithostratigraphy

The Ashin Formation in the area under study has a thickness of 330m and is characterized by an erosive contact with the underlying Baqoroq Formation. Most of the Baqoroq Formation is composed of coarse-grained conglomerate. The Ashin Formation encompasses interbedded sandstone, shale, calcareous sandstone, and limestone (Fig 3).

Fig 3. a) View of the sandstone layers of the middle part of the Ashin Formation b) View of the middle part of Ashin Formation c) View of the upper part of Ashin Formation d) View of the sandstone layers at the top of the Ashin Formation

Most of the thickness of the Ashin Formation is related to shale and sandstone and the thickness of other facies is limited (Fig 4a). The most frequent sedimentary structure in the Ashin Formation is parallel lamination and cross-bedding in medium to thin-bedded sandstone and limestone (Fig 4b-c). In addition, ripple-cross stratification and convolute lamination are present (Fig 4 d-e).

Other features of the Ashin Formation include numerous fractures which are often filled by iron oxide belonging to late stage diagenesis. In some areas, the sandstone bed of the Ashin Formation are lens-shaped and laterally disrupted. These sandstone beds exhibit ripple cross-lamination (Fig 4f and Fig 5). Other features of the Ashin deposits include ichnofacies such as Ctenopholeus, Paleodictyon, Lorenzinia, Megagrapton and Protopaleodictyon, which were all identified in the

studied exposure of the Ashin Formation. Ctenopholeus ichnofacies is not a useful indicator for determining sedimentary environments since it is found in both deep and shallow water facies (Seilacher 2007) (Fig 6a). However, the presence of Nereites trace fossils (Paleodictyon, Lorenzinia, Megagrapton and Protopaleodictyon) indicates a deep marine origin for the Ashin Formation (Fig 6b and Fig 7a-d). Low-oxygen environments and sedimentation via turbidity currents are characteristic of the Nereites ichnofacies (Seilacher 2007). Other fossils observed in sandstone facies of studied section include bivalves and echinoderms (Fig 7e-f).

5. Constituent facies in Ashin Formation

The stratigraphy of the Ashin Formation is composed of sandstone, shale and limestone facies. The facies and microfacies constituting this formation are introduced below.

5.1. Sandstone facies

The brown to dark gray sandstone facies represent around 75 m of the thickness of the Ashin Formation in the studied section. Parallel and cross-bedding is commonly observed in this facies. Sandstone beds are medium to thin-bedded and are interbedded with shale. Microscopic study of thin sections of sandstones has led to the identification of the following fine facies.

5.1.1. Graywacke

This petrofacies can be identified with abundant matrix (more than 15%). Most of the particles consist of monocrystaline quartz Grain sorting ranges from medium to poor and the particles are angular to semi-angular. In addition to quartz, lithic fragments are also found in these facies. The amount of lithic fragments in this petrofacies is more than plagioclase and fine mica . blades. The high matrix frequency makes the particles observed as floating in the matrix. According to the classification of Pettijohn et al. (1987), these petrofacies are of the graywacke to lithic wacke type (Fig 8a).

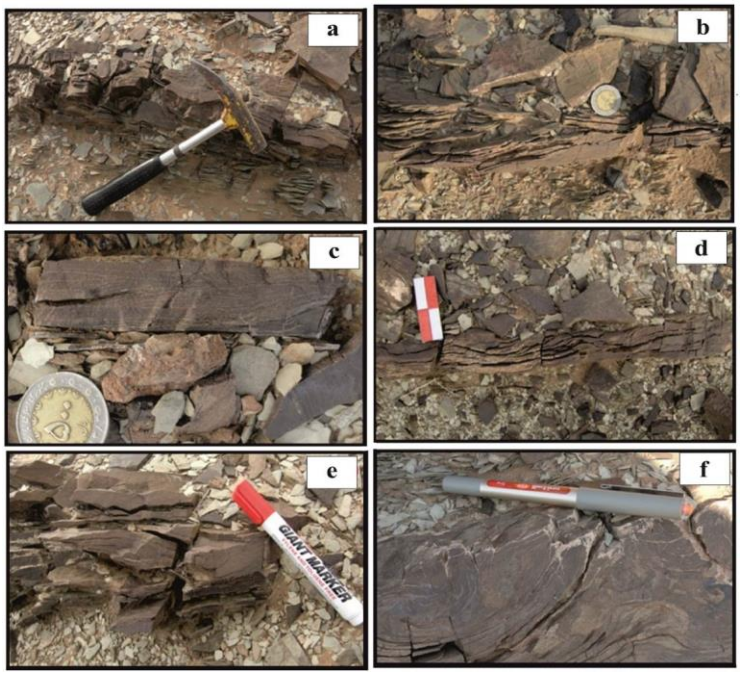

Fig 4. a) The alternation of sandstones and mudstones that form the largest part of the Ashin Formation, b) Cross- lamination in sandstone, c) Parallel and cross- lamination in sandstone, d) ripple-cross lamination in the sandstone, e) Convolute lamination in sandstone, f) Ripple-cross lamination in lens-shaped sandstone.

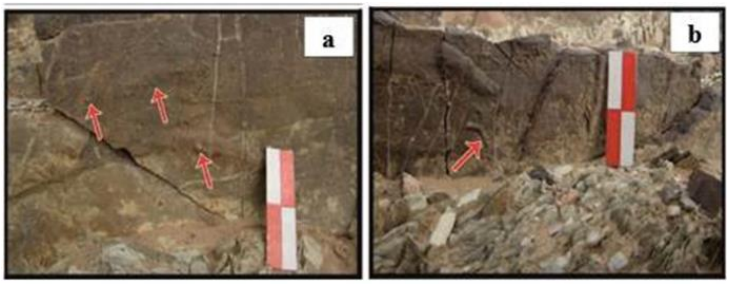

Fig 5. a) Sandstone facies with parallel and cross- lamination structures. b) Interbedded sandstone and shale facies. c) Carbonate facies with parallel lamination d) Lens-shaped sandstone layer (laterally interrupted)

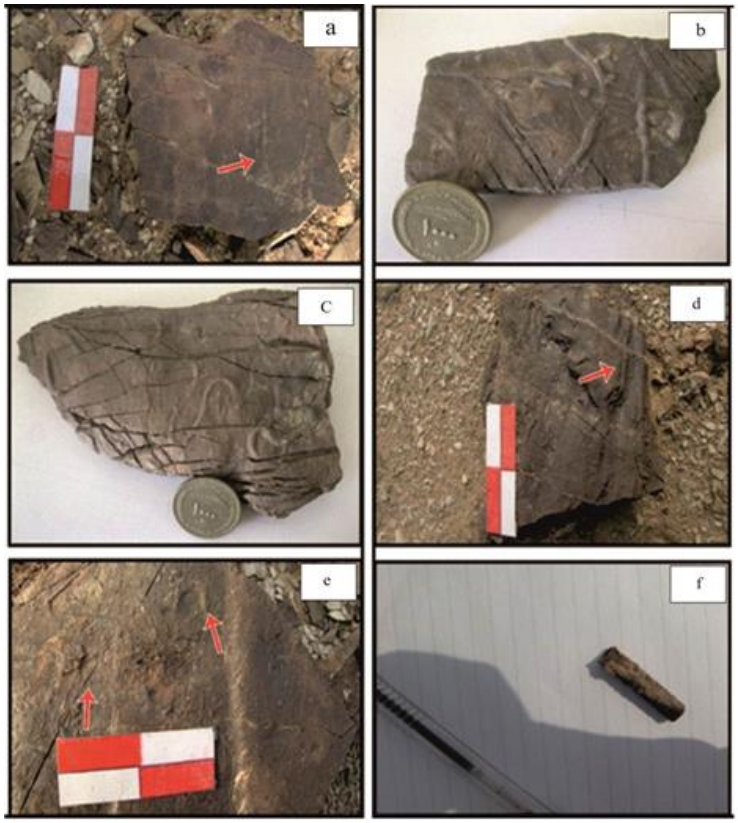

Fig 6. a) trace fossils of Ctenopholeus ichnophyses, and b) Remnants of the Paleodictyon trace fossil.

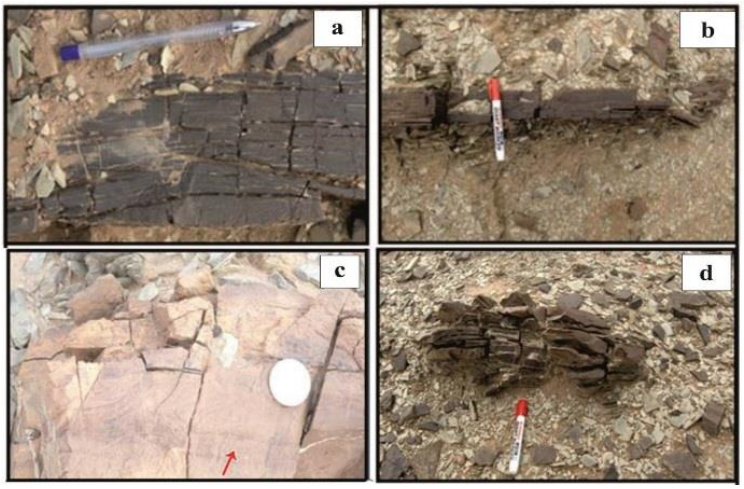

Fig 7. Types of trace fossils found in the deposits of the Ashin Formation: a) Echinophas Lorenzinia isp belonging to Nereites facies, b) Megagrapton echinophasis of the Nereites facies, c) Protopaleodictyon isp belonging to Nereites facies, d) Megagrapton's, e) Bivalve fossil on sandstone of Ashin Formation, and f) Echinoderm fossils found in the Ashin Formation.

5.1.2. Litharenite

Litharenite are sandstones with less than 95% quartz and the amount of lithic fragments (more than 25%) is greater than that of feldspar. Lithic fragments identified in the studied sandstones include sedimentary, volcanic and carbonate rocks. Based on Folk's (1980) classification, this petrofacies is chert-arenite due to the large amount of chert detritus. Quartz content in this petrofacies is about 65-70%. Monocrystalline quartz is more abundant than polycrystalline types. However, polycrystalline quartz accounts for almost 5% of this petrofacies. In addition, most of the observed cement is composed of silica, although hematite and dolomitic cement is also found to a lesser extent. Both types of feldspar grains (K-Feldspars and plagioclase) are also found. Most feldspar is affected by sericitation and is altered. Some unweathered plagioclase is present in the sandstone. In addition to chert fragments, volcanic and metamorphic rocks fragments are also present to a lesser extent in these facies. Most metamorphic lithic fragments are slate and

phyllite. Heavy minerals present are often zircon grains, (which are usually found in semi-rounded shapes and in small amounts, around 1%). The effects of severe weathering are abundant in this petrofacies, often filled with iron oxide. The presence of calcite-filled veins is another feature of the petrofacies (Fig 8b- c).

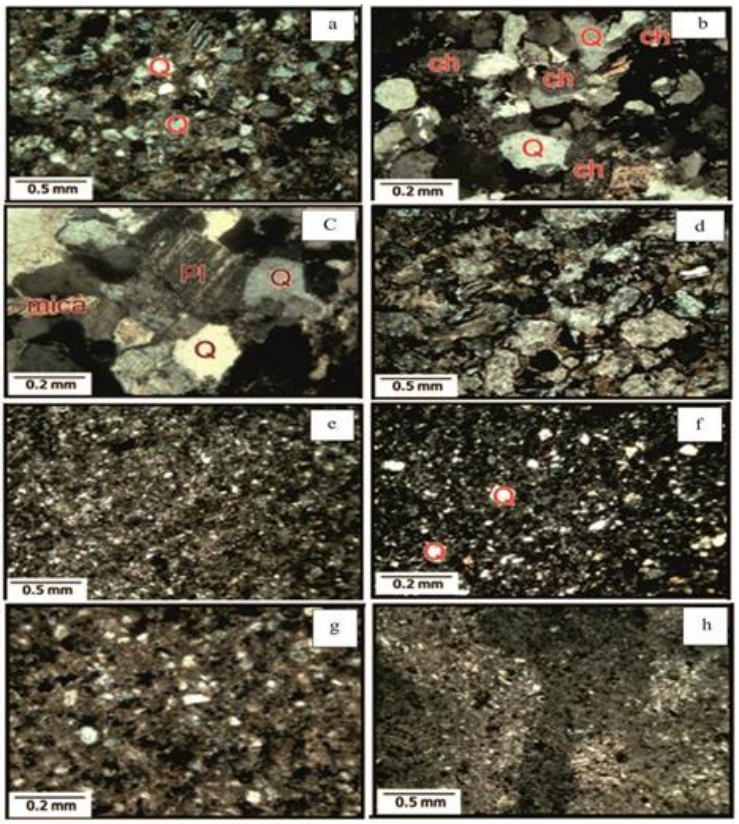

Fig 8. a) Graywacke petrofacies with fine-grained crumbs (XPL light), b) Litharenite petrofacies with chert crumbs and silica cement (light) (XPL), c) Altered plagioclase grain in litharenite petrofacies (XPL light), d) Medium to fine-grained Calclithite fine-grained facies (light) XPL), e) Classic siltstone petrofacies (XPL light), f) Siltstone petrofacies (XPL light), g) Limy siltstone petrofacies (XPL light), and h) Lime Mudstone microfacies (XPL light).

5.1.3. Calclithite

This petrofacies is identified as light gray to brown coloured with a thickness of 26 m. This petrofacies is observed in the upper parts of the section as medium- to coarse-grained deposits. The bulk of this petrofacies is composed of carbonate detritus. The sorting is moderate and the particles are semi-angular to semi-rounded. The effects of micritization on carbonate particles is detectable. The amount of compaction in this microfacies is approximately moderate and the cement formed is mostly iron oxide belonging to late stage diagenesis. In addition to carbonate fragments, volcanic detritus can be observed in less than 5% of these petrofacies. Moreover, sedimentary detritus (chert and sandstone) are found to a very small extent. because of the to the abundance of sedimentary rock fragments and based on Folk's classification (1980), this petrofacies is calclithite type due to the high amount of carbonate detritus (Fig 8d).

5.1.4. Claystone facies

The claystone facies is abundant in the Ashin Formation and represents the largest part of its thickness. Based on x-ray diffraction analysis (Fig 9), this facies mainly contains quartz, sheet silicates, plagioclase and calcite as major constituents, and gypsum as minor constituent phases. In addition, observed clay minerals in the studied shale is mainly illite and kaolinite.

5.2. Siltstone facies

5.2.1. Classic siltstone

This petrofacies mainly consists of monocrystalline quartz grains and mica blades. In some cases, mica blades have a certain orientation. Classic siltstone shows lamination. The darker layers are mainly composed of clay-sized particles, while the lighter layers are composed of transparent quartz (Fig 8e).

5.2.2. Sandy siltstone

In this petrofacies, the sand content fluctuates between 10 and 50%. The sand grains are mainly composed by monocrystalline quartz (Fig 8f).

5.2.3. Limy siltstone

Similar to the classical siltstone, petrofacies includes single-crystalline quartz and mica blades. Of course, the mica content in these petrofacies is lower. This

petrofacies is recognizable by its calcareous content (about 10 to 20%) (Fig 8g).

5.3. Limestone facies

This facies has a light brown colour and is observed interbedded with shale and sandstone, with a general thickness of 6.5 m. Parallel lamination is the only sedimentary structure observed in this facies. The study of thin sections in the laboratory led to the identification of the following microfacies.

5.3.1. Lime Mudstone

This fine-grained carbonate microfacies lacks allochems. Very fine clam shells can be observed. The lime mudstone microfacies is observed intercalating with silicate sediments. (Fig 8h).

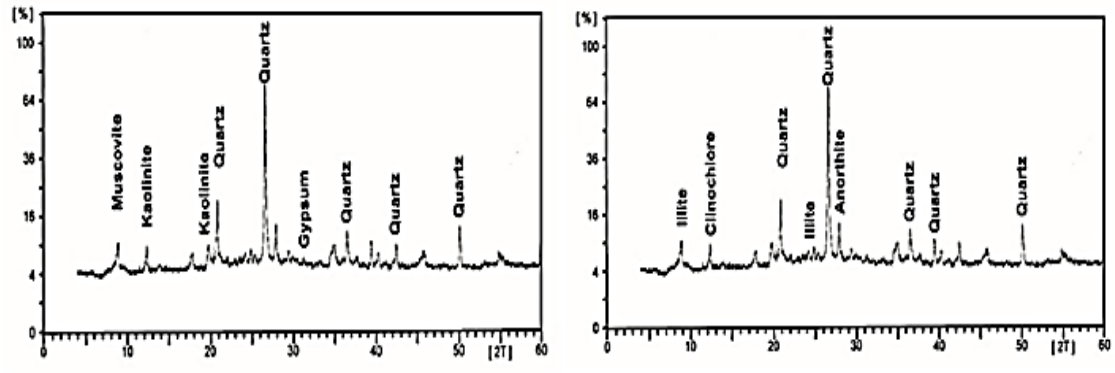

Fig 9. X-ray diffraction pattern (XRD) of two samples of the Ashin Formation shales.

6. Sedimentary environment

The Ashin Formation in the studied southern section of the Nakhlak mine include sandstone, mudstone, and limestone facies. Sedimentary structures include parallel-bedding, cross-bedding, convolute-bedding, and ripple cross lamination. The stratigraphic column and the observed facies are illustrated in Fig 10. These facies can be sub-divided into limestone and clastic facies sets. The limeston facies contain the lime mudstone microfacies. This microfacies is related to pelagic carbonates intercalated with sandstone and shale sediments. The clastic facies set of the Ashin Formation consists of alternating sandstone and shale with parallel-bedding, cross-bedding, convolute-bedding and slumping structures. In addition to sedimentary structures, the ichnofossil assemblages identified in the Ashin Formation include Paleodictyon, Lorenzinia, Megagrapton, and Protopaleodictyon trace fossils, representing a deep marine origin associated with the Nereites facies. The Nereites facies are formed with in sediments on the continental slope to the abyssal plain. Some layers of sandstone in the Ashin Formation are lens-shaped and have low lateral continuity. This pattern of deposition indicates the deposition of sandstones in deep-sea submarine channels (Tudor 2014; Van der Merwe et al.2014;Brooks et al.2018;). Parallel layering in the sandstone beds seems to represent the Tb division of the Bouma sequence (Bouma 1962) and the rippled beds Tc division of the sequence. In these facies sets, petrofacies alternation of graywacke, litharenite and calclithite is observed with shale facies. The study of sedimentary structures, fossil records, and lateral and vertical relationships between the facies of the Ashin Formation indicates that the limestone facies assemblage was deposited in the more proximal parts of the distal submarine fan, sandstone facies are deposited in the middle parts of the distal submarine fan, and shale facies are deposited in the outer part of the distal submarine fan.According to Stow (2005), if the ratio of sandstone to shale is high, it indicates that sediment have been deposited at the inner lobe, the equal ratio of sandstone to shale indicates deposition of sediments in the middle lobe part, and finally low ratio of shale to sandstone indicates outer lobe sediments. According to the facies column of the Ashin Formation, the ratio of shale to sandstone is high therefore reflecting deposition in the distal parts of the submarine fan (distal fan).

With respect to the column of the facies attributed to Ashin formation, the ratio of shale to sandstone is high and represents deposition in an outer lobe and distal submarine fan setting. According to the classification of Reading and Richards (1994) and Nichols (2009), the submarine fan of the Ashin Formation was probably a compound fan of sand and shale with a higher shale contents. Fig 11 illustrates the sedimentary model presented for the Ashin Formation.

7. Geochemical studies

7.1. Petrography of siliciclastic deposits of the Ashin Formation

Based on grain-size classes, siliciclastic deposits of the Ashin Formation can be divided into medium- and fine-grained deposits. These sandstones contain quartz, lithic fragments, mica and heavy mineral grains. These grains are angular to semi-angular with moderate to weak sorting. The modal composition of these sandstones is illustrated in Table 1.

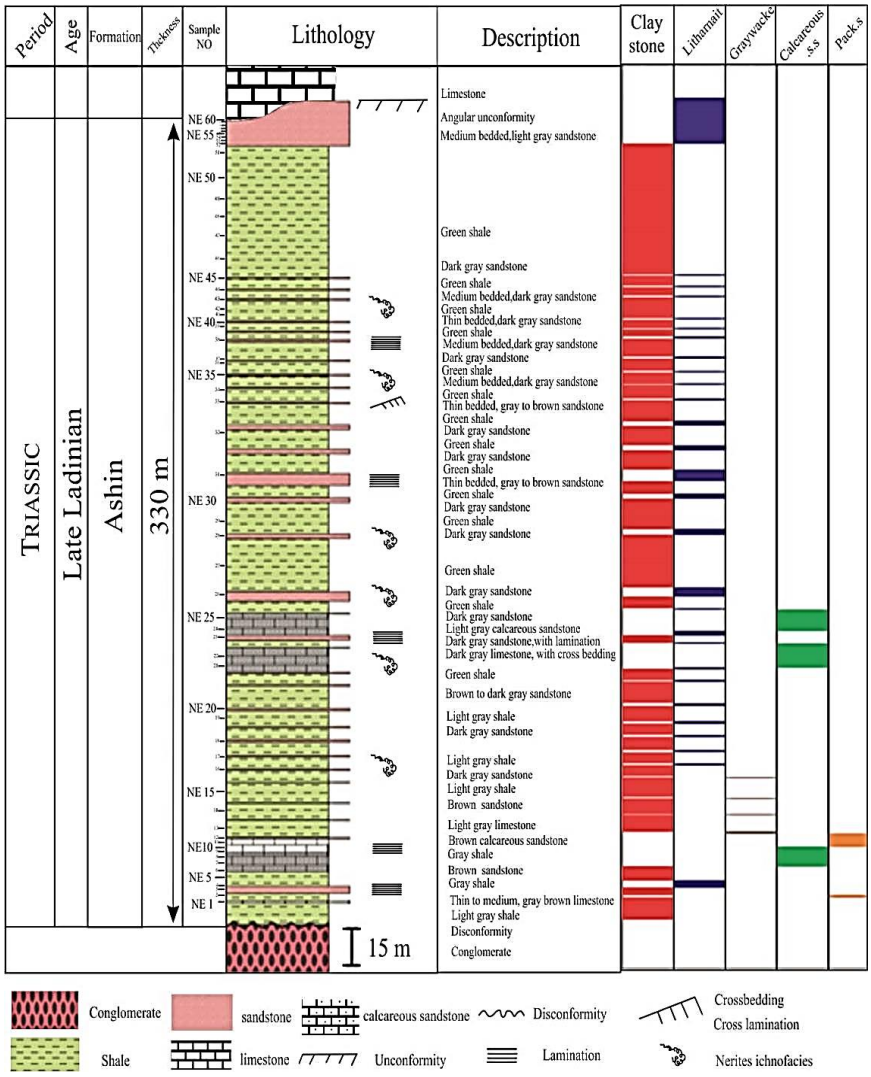

Fig 10. Stratigraphic column of the Ashin Formation in the studied section.

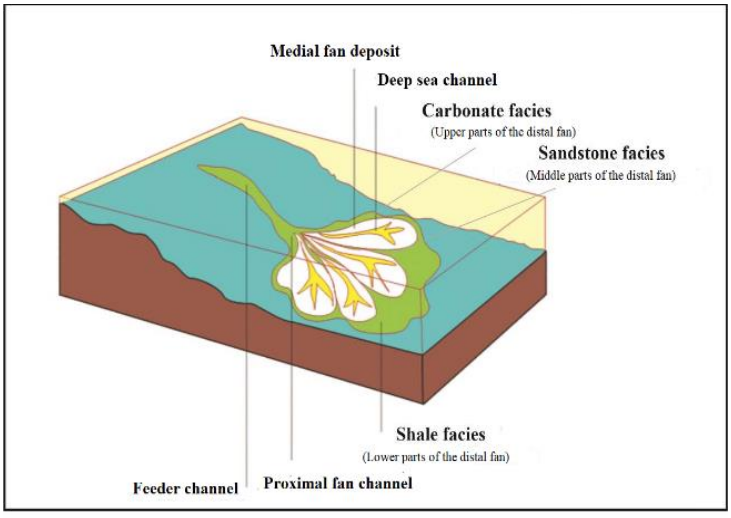

Fig 11. Sedimentary model presented for the Ashin Formation.

Quartz is the most abundant mineral, consisting mainly of monocrystalline (65%) with wavy extinction and polycrystalline (5%) types. Feldspars are found in both plagioclase and alkaline varieties and constitute 6% of the clastic constituents of these sandstones. lithic fragments are mainly composed by volcanic, sedimentary, and metamorphic types which account for 29% of the clastic grains. Sedimentary lithic fragments are predominantly chert, carbonates (crushed fossil fragments) and shale. Metamorphic fragments are slate and slate-like fossils. Volcanic fragments contain thin, elongated feldspar crystals of glassy texture. In addition, micas and heavy minerals, such as muscovite and zircon are found in some sections. With respect to the percentage of constituents and according to Folk's (1980) classification, the studied sandstones can be classified as litharenites, feldspathic litharenites and sublitharenites (Fig 12).

Table 1. Modal composition (%) of sandstone samples of the Ashin Formation

Sample No.	Qm	Qp	Qt	F	L	Lt
NE.12	67	0	67	5	28	28
NE.23	70	0	70	5	25	25
NE.26	60	0	60	8	32	32
NE.28	67	0	67	8	25	25
NE.30	75	0	75	2	23	23
NE.31	56	10	66	12	22	32
NE.38	69	11	80	7	13	24
NE.40	78	0	78	6	16	16
NE.43	68	6	74	4	22	28
NE.45	73	3	76	2	22	25
NE.52	48	15	63	8	29	44
NE.57	55	8	63	4	33	41
NE.60	61	7	68	6	29	33

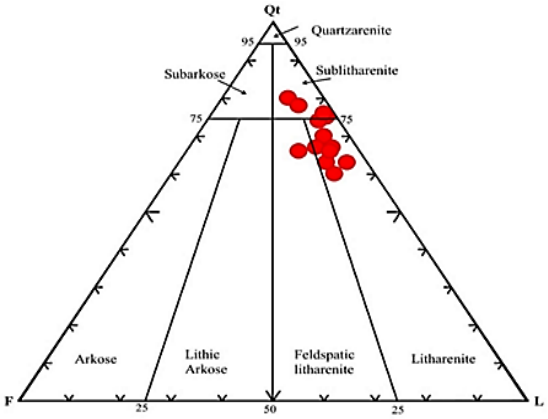

Fig 12. Compositional classification of studied sandstone samples from the Ashin Formation based on Folk (1980).

7.2. Geochemical classification of siliciclastic deposits of the Ashin Formation

In addition to petrographic studies, data from geochemical analysis of the major elements were plotted on the geochemical classification diagram of Pettijohn et al. (1987) and their petrographic classification (as litharenite and sublitharenites) was confirmed (Fig 13a). Furthermore, major element data from XRF analysis of sandstones were also plotted on the classification diagram of Herron'(1988) and the petrographic classification of these sandstones was again confirmed (Fig 13b). It seems that the presence of hematite cement in some samples caused them to be classified as Fe-sand in Herron (1988) diagram. In addition, the plotting of shale samples in Herron (1988) diagram classifies them as of iron-free shales (Fig13b). The geochemical classification results seem to validate previous petrographic classification.

7.3. Major element oxide contents of siliciclastic deposits of the Ashin Formation

The major elements are often limited to the ten elements which are expressed as oxides in chemical analysis (Si, Al, Ti, Fe, Mn, K, Mg, Ca, Na, P) (Rollinson 1993). Some information on tectonic setting and source of sediment can be obtained through these elements and their plot design (Roser and Korsch 1986). Tables 2 and 3 indicate the results of major elements contents of the clastic deposits of the Ashin Formation. As shown in Table 2, the average silica content in sandstone is larger than in shale samples, which indicates the abundance of quartz and chert grains in sandstone. The mean of Na_2O, MnO and CaO in sandstone is higher than that of shales and the mean of Al_2O_3, MgO, K_2O, Fe_2O_3, TiO_2 and P_2O_5 in shale is more than that of sandstone. High Al_2O_3, TiO2 and K_2O levels in shales may be related to illite and muscovite presence (Lopez et al. 2005). The K_2O / Al_2O_3 ratio in the shales of the Ashin Formation ranges between 0.12 to 0.22 with a mean of 0.17, which probably indicates that clay minerals present are controlled by the relative frequency of kaolinite and illite (Ghosh and Sarkar 2010). The Na_2O content is about 1.73% in sandstone, and 1.36% wt in shale indicating the presence of sodium plagioclase and clay minerals.

The amounts of MgO and CaO are related to calcareous grains, dolomitic cements, and diagenesis of plagioclase, Fe2O3 content is related to the presence of hematite cement and clay minerals (McLennan et al. 1983; Nath et al. 2000; Zhang 2004; Osae et al. 2006). Based on UCC normalization diagrams, it is specified in what extent the deposit's composition is resembling with upper continental crust indicating enrichment or depletion. This method is considered as one of the most commonly used (Taylor and McLennan 1985; Rollinson 1993) since the chemical composition of the upper crust is an important feature in understanding the composition and difference of continental crust chemistry around the world (Rudnick and Fountain 1995; Taylor and McLennan 1985). Figure14 displays the UCC-normalized pattern for the sandstone and shale samples of the Ashin Formation. Observed CaO enrichment in sandstone samples is probably due to the presence of carbonate grains, calcite and dolomitic cement, as well as plagioclase diagenesis. Depletion can be observed in sandstone samples for MgO, as well as in both shale and sandstone samples for MnO and P2O5. The depletion of MgO in sandstones can be attributed to its high mobility during chemical weathering, diagenesis and secondary alteration (Das et al. 2006; Mclennan 2001). In addition, other elements are within the UCC range.

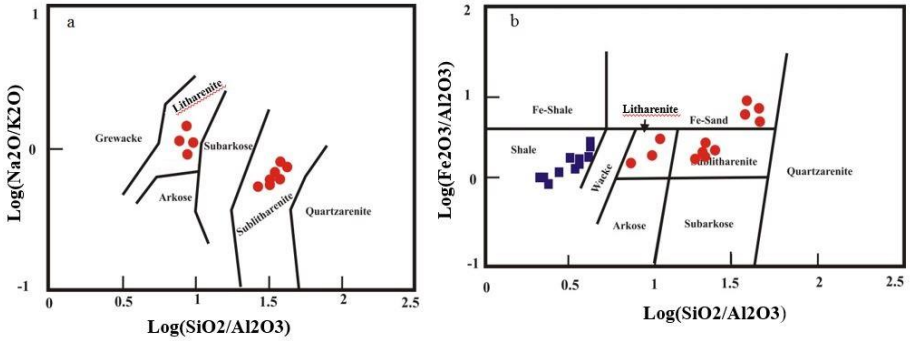

Fig 13. a) Geochemical classification of sandstones based on Pettijohn (1987), sandstone samples of the Ashin Formation fall within the litharenite and sub-litharenite ranges, and b) Classification of sandstones and shales based on Herron (1988), sandstones of the Ashin Formation fall within the range of litharenite, sub-litharenate, and Fe-sand.

Table 2. Percentage of major oxides and percentage of loss on ignition (LOI) in sandstones of the Ashin Formation.

Sample No.	SiO_2	Al_2O_3	Na_2O	MgO	K_2O	TiO_2	MnO	CaO	P_2O_5	Fe_2O_3	LOI	ICV
NE.12	52.08	7.80	2.09	0.99	0.86	0.40	0.50	18.88	0.08	3.71	12.28	3.15
NE.23	49.15	7.42	1.70	1.47	0.73	0.40	0.47	19.52	0.06	4.74	14.18	3.19
NE.26	57.84	7.26	1.64	1.54	0.63	0.43	0.43	14.11	0.07	5.49	10.37	3.34
NE.28	60.78	7.81	1.78	1.87	0.55	0.46	0.37	11.61	0.07	5.54	9.03	2.83
NE.30	64.18	9.52	1.42	2.22	1.08	0.53	0.22	6.60	0.09	6.96	7.05	1.99
NE.31	67.17	8.90	2.17	1.70	0.69	0.54	0.19	6.92	0.08	5.63	5.90	2.00
NE.38	77.89	8.10	3.08	0.94	0.40	0.40	0.07	2.90	0.04	3.48	2.60	1.39
NE.40	73.10	8.82	2.48	1.41	0.66	0.48	0.10	3.79	0.07	5.28	3.69	1.60
NE.43	66.25	8.50	1.83	0.89	0.67	0.41	0.12	8.96	0.07	4.98	7.18	2.10
NE.45	63.73	7.04	1.82	0.74	0.55	0.36	0.24	11.93	0.06	4.72	8.71	2.89
NE.52	83.01	8.45	1.12	0.22	1.07	0.19	0.08	1.44	0.02	2.10	2.23	0.73
NE.57	78.14	7.35	1.07	0.65	0.80	0.19	0.09	4.68	0.02	2.50	4.31	1.35
NE.60	77.28	10.51	0.33	0.32	1.24	0.21	0.07	3.69	0.02	2.04	4.20	1.35
Average	67	8.26	1.73	1.15	0.76	0.38	0.22	8.84	0.05	4.4	7.05	2.18

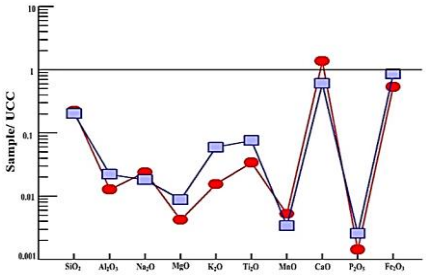

Fig 14. UCC-normalized plot for the sandstone and shale samples of the Ashin Formation (Taylor and McLennan 1985) (solid red circle = sandstone samples, solid blue square = shale sample).

7.4. Tectonic setting of siliciclastic deposits of the Ashin Formation

A large number of studies have been conducted to investigate the relationship between the chemical composition of sedimentary rocks and their source area (e.g., Cullers 2000; Alvarez and Roser 2007; Manikyamba et al. 2008; Spalletti et al. 2008; Akarish and El-Gohary 2008; Paikaray et al. 2008; Dey et al. 2009; Mishra and Sen 2010). Determining the tectonic setting of sandstones through the use of rock framework minerals (modal analysis) was first proposed by Crook (1974) and then underwent significant changes by Dickinson and Suczek (1979) and Dickinson et al. (1983) by identifying the relationship between sandstone composition and important types of settings such as stable cratons, basement uplifts, magmatic arcs, and recycled orogens. The modal analysis is the result of counting the grains of the stone framework. The modal analysis of the Ashin Formation sandstones was plotted on QtFL and QmFLt triangular diagrams (Dickinson et al. 1983). Both diagrams illustrate the same trend and the tectonic setting of the sandstones of the Ashin Formation is defined as of a recycled orogen (Fig 15a-b). As shown previously, the presence of sedimentary detritus in the studied thin sections confirms the above result. Low percentages of unstable grains such as feldspars, high abundance of monocrystalline quartz grains (Qm), and alteration of feldspar grains indicate that the source area is affected by severe chemical weathering and hot humid weather (Pettijohn et al. 1987; Amireh 1991).

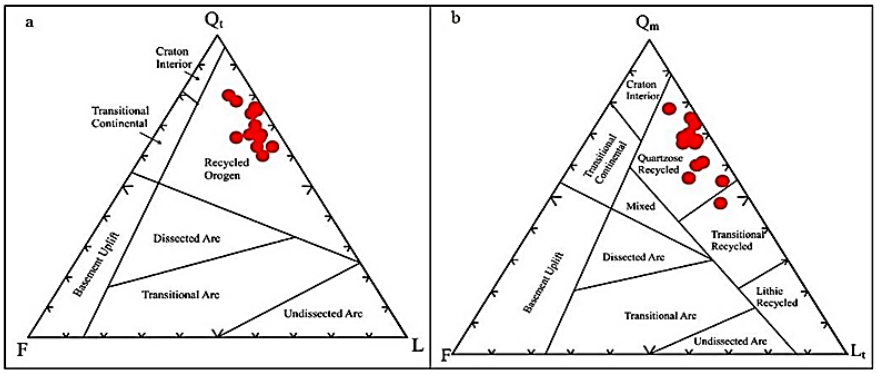

Fig 15. Provenance of sandstones of the Ashin Formation based on the a) QtFL and b) QmFLt triangular diagrams of Dickinson et al (1983).

The tectonic setting of sandstones can be also determined through the percentage of major elements (Schwab 1975; Bhatia 1983; Roser and Korsch 1986 and 1988; Armstrong-Altrin et al. 2004). Battia (1983) and Roser and Korsh (1986 and 1988) used tectonic discrimination diagrams in many cases to determine the tectonic setting of unknown basins (Jafarzadeh et al. 2013; Nowrouzi et al. 2013). Bhatia (1983) illustrates four different tectonic settings including oceanic island arc (A), continental island arc (B), active continental margin (C), and passive continental margin (D). Plots of shale and sandstone data from the Ashin Formation on this diagram illustrate their tectonic setting on the active continental margin field (Fig 16a). The diagram of Maynard et al. (1982) uses elemental ratios of SiO2 / Al_2O_3 versus K_2O / Na_2O and separates passive margin (PM) from active continental margin (ACM) and
magmatic arc (A1 and A2) sediments. Shale and sandstone data of the Ashin Formation plot on the acidic-intrinsic arc (A2) and also on the active continental margin (ACM) field of this diagram (Fig 16b). A new discriminant-function multi-dimensional diagram proposed by Verma and Armstrong-Altrin (2013) has been also used to identify the tectonic setting of the Ashin Formation (Fig 17). This diagram is divided into three main fields (arc, collision and rift) based on the two discrimimant functions that use the major element abundances (SiO_2, TiO_2, Al_2O_3, CaO, Na_2O, K_2O, MnO, MgO, P_2O_5, and Fe_2O_3). Verma and Armstrong-Altrin (2013) proposed two diagrams, one for clastic sediments with high-silica content (95%≥ SiO_2> 63%) and another for clastic sediments with low-silica content (63%≥ SiO_2> 35%). All the shale and sandstone samples of Ashin Formation were plotted on the arc field for both high- and low-silica samples (Fig 17).

7.5. Provenance of Ashin Formation shale

Elements such as Ti, Al, and Zr are usually transported as solid particles, which are less affected by weathering, metamorphic and diagenetic processes due to the low solubility of oxides and hydroxides of these elements in low-temperature aqueous solutions. Therefore, they are considered as more reliable for use in provenance studies (Taylor and McLennan 1985).The ratio of Al_2O_3 / TiO_2 oxides in shale is a good indicator for interpreting their source rock (Schieber 1992; Hayashi et al. 1997; Paikaray et al. 2008). Al_2O_3 values in the shale of the Ashin Formation range from 8.98 to 18.11% with a mean of 14.36%, while TiO_2 values range between 0.46 and 0.84% with a mean of 0.67%. The Al_2O_3 / TiO_2 ratios for shale samples of the Ashin Formation show intermediate to granite parent rocks for these shales (Fig 18).

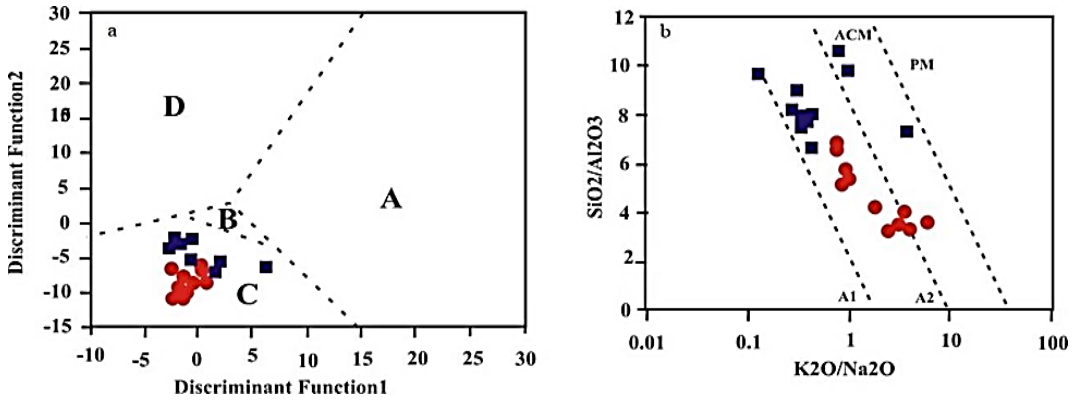

Fig 16.a) Tectonic setting diagram of Bhatia (1983) using major element oxides. The diagram illustrates four tectonic settings including oceanic island arc (A), continental island arc (B), active continental margin (C), and passive continental margin (D). Shale samples (blue square) and sandstones (red circle) of the Ashin Formation were classified as active continental margin sediments b) The tectonic setting diagram of Maynard et al. (1982), which represents passive margin (PM), active continental margin (ACM), and magmatic arc (A_1 and A_2) fields. Shale samples (blue square) and sandstones (red circle) of the Ashin Formation plotted on the active continental margin field.

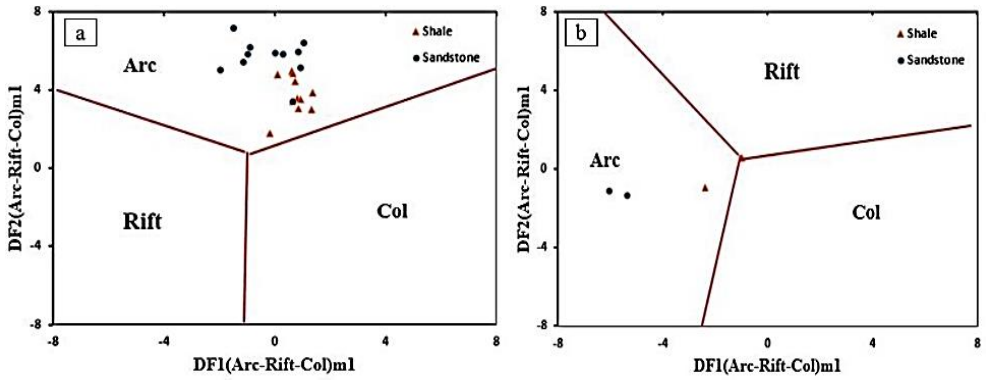

Fig 17. a) Discriminant-function multi-dimensional diagram for high-silica clastic sediments from three tectonic settings (arc, continental rift, and collision) b) discriminant-function multi-dimensional diagram for low-silica clastic sediments from three tectonic settings (arc, continental rift, and collision) (Verma and Armstrong-Altrin, 2013)

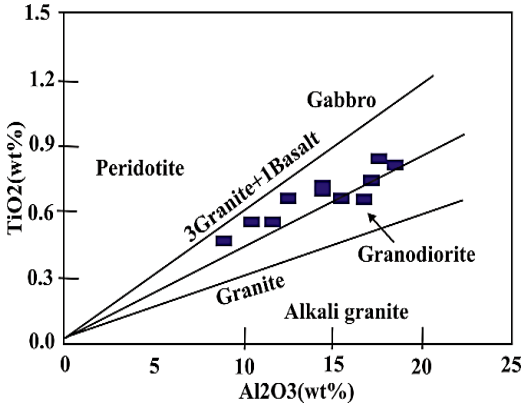

Fig 18. Al_2O_3 / TiO_2 oxides ratio (Schieber 1992) for the studied shales of the Ashin Formation (blue square).

The positive correlation of Al_2O_3 with K_2O (r = 0.97), Na_2O (r = 0.64) and MgO (r = 0.24) in the studied shale (Fig19a-c) indicates that the concentration of potassium minerals such as illite and muscovite have little effect on Al distribution (McLennan et al. 1983; Jin et al. 2006). The K_2O / Al_2O_3 ratio can be used as an indicator to determine the main composition of shales (Lee 2002). This ratio was different for clay minerals and feldspars so 0-0.3 for clay minerals and 0.3-0.9 feldspars (Cox et al. 1995).

Table 3. Percentage of major element oxides and loss of ignition (LOI) for the shales of the Ashin Formation.

Sample No.	SiO_2	Al_2O_3	Na_2O	MgO	K_2O	TiO_2	MnO	CaO	P_2O_5	Fe_2O_3	LOI	ICV	K_2O/Al_2O_3
NE.2	61.58	15.48	1.00	2.31	3.51	0.66	0.10	2.55	0.06	6.73	5.83	1.08	0.04
NE.5	55.69	16.54	1.48	2.35	3.64	0.66	0.20	4.72	0.06	6.91	7.53	1.20	0.03
NE.15	60.06	14.61	1.47	2.65	2.62	0.72	0.11	3.71	0.10	7.49	6.29	1.28	0.04
NE.19	59.91	18.11	1.07	3.06	4.13	0.82	0.05	0.68	0.13	7.55	4.29	0.95	0.04
NE.29	61.21	14.61	1.45	2.76	2.62	0.70	0.16	3.41	0.10	6.67	6.13	1.21	0.04
NE.32	65.17	12.55	1.82	2.40	1.53	0.67	0.12	2.90	0.12	7.79	4.79	1.37	0.05
NE.34	61.31	17.86	1.29	2.70	4.03	0.84	0.06	0.57	0.11	5.93	5.12	0.86	0.04
NE.36	60.57	10.61	1.57	2.09	1.53	0.56	0.19	7.94	0.08	6.87	7.85	1.95	0.05
NE.46	60.15	8.98	1.51	1.81	1.12	0.46	0.21	10.29	0.07	6.65	8.62	2.48	0.05
NE.48	62.41	11.49	1.62	2.43	1.51	0.56	0.15	5.45	0.08	7.72	6.43	1.69	0.04
NE.50	61.83	17.17	0.69	1.09	3.81	0.74	0.08	1.51	0.10	6.66	0.00	0.84	0.04
Average	60.9	14.35	1.36	2.33	2.73	0.67	0.13	4	0.09	7	6.27	1.36	0.04

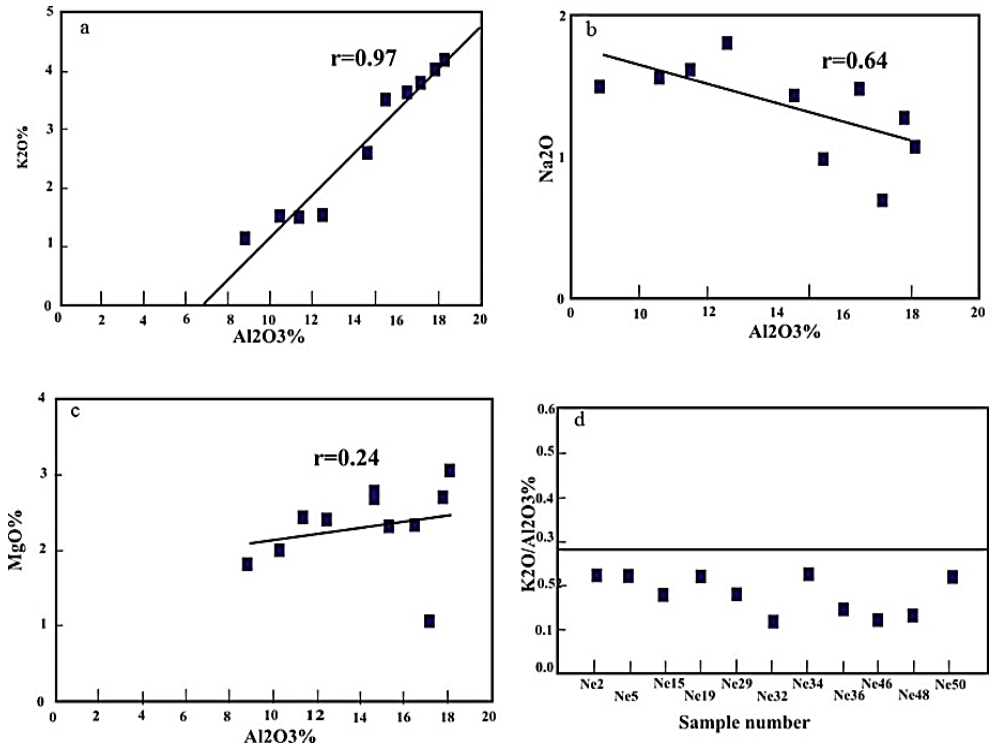

Fig 19. Correlations of K2O (a), Na2O (b) and MgO (c) with Al2O3 and K2O / Al2O3 (d) ratio (Lee 2002) for the shales of the Ashin Formation (blue filled square).

The average K_2O / Al_2O_3 ratio in the shales of the Ashin Formation is 0.04 (Table 3), indicating the presence of potassium minerals in these shale (Cox et al. 1995) and plotting the K_2O / Al_2O_3 ratio for the shale samples of the Ashin Formation indicates a parent rock of intermediate to granite composition for these shales (Fig 19d).

7.6. Weathering of siliciclastic deposits of the Ashin Formation

The weathering history of ancient sedimentary rocks can be accessed through examining the relationships between alkali and alkaline earth elements (Nesbitt and Young, 1982). The chemical weathering intensity of the source rocks is mainly controlled through the source rock composition, weathering, climatic conditions and tectonic uplift of the source area (Wronkiewicz and Condie 1987). Almost 75% of the upper crustal remnants are composed of feldspars and volcanic rocks whose chemical weathering results in the formation of clay minerals (Nesbitt and Young 1984 and 1989; Taylor and McLennan 1985; Fedo et al. 1995). The rate of rock chemical weathering can be evaluated through proposed geochemical indexes such as the Chemical Index of Alteration (CIA) (Nesbitt and Young 1982), Plagioclase Index of Alteration (PIA) (Fedo et al. 1995), Chemical Index of Weathering (CIW) (Harnois 1988), and CIW′

(Cullers 2000). The CIA index is obtained from the following equation (1):

$$CIA = [Al_2O_3 / (Al_2O_3 + CaO^* + Na_2O + K_2O)] \times 100 \quad \text{(Equation 1)}$$

where CaO* is the amount of CaO in the silicate part of the rock and the amount of major oxides is based on the molecular ratio. Specimens with CaO greater than 5% are not considered to determine the exact amount of CIA and eliminate the influence of diagenetic cements on CaO content (Garcia et al. 2004).

CIA index for sampled sandstones and shales of the Ashin Formation (except for samples with a CaO content above 5%) ranges from 52.87-69.95 (mean= 60.28), and 62.69-75.48 (mean= 69.27) (Table 4), respectively, indicating moderate to low weathering of the source area. Since the samples with high CaO reduce the CIA mean and should be eliminated from the data, the CIW' weathering index was also calculated for the Ashin Formation data. This index is obtained from equation (2):

$$CIW' = [Al_2O_3 / (Al_2O_3 + Na_2O)] \times 100 \quad \text{(Equation 2)}$$

where the amount of major oxides is based on the molecular ratio.

Changes in CIW' index for sampled sandstones and shales of the Ashin Formation are 72.45-96.95 (mean= 82.82) and 85.48-96.16 (mean= 90.81), respectively (Table 4), which indicates severe weathering of the source area under warm and humid climatic conditions

Use of the QFRf triangular diagram of Suttner et al. (1981) indicates a source area composed of metamorphic rocks within a humid climate (Fig 20). This diagram only illustrates the metamorphism and internal igneous rock provenance (under wet or dry climatic conditions) and does not display different tectonic settings. Sandstone data classification under the diagram of Weltje et al. (1998) (Fig 21) illustrates that these sandstones have a weathering coefficient within the range of 0 and 1 indicating an area of metamorphic and igneous rock provenance, of high to medium relief, and Mediterranean to semi-humid climate. On a SiO2 percentage versus total percentage of $Al_2O_3 + K_2O + Na_2O$ diagram (Sutner and Datta 1986), Ashin Formation samples seem to be plotted at the areas indicate dry to semi-humid climatic conditions with high chemical maturity (Fig 22).

Weathering trends can be also obtained by using the A-CN-K triangle (Nesbitt and Young, 1984; Fedoet al, 1995). On this diagram, the initial stages of weathering will have a parallel trend to the A-CN side. However, during advanced weathering, as the compounds move toward vertex A, there is a marked decrease in K_2O (Nesbitt and Young et al, 1984). The samples of Ashin Formation are generally parallel to the A-CN side and in the early stage of weathering. These samples show a trend from basalt and andesite to weathered dacite (Fig 23).

Table 4. CIA (Chemical Alteration Index) and CIW (Weathering Alteration Index for Carbonate-bearing clastic rocks) indices calculated for sandstone and shale samples of the Ashin Formation.

Sample No.	CIA	CIW'	Sample No.	CIA	CIW'
NE.12	-	78.86	NE.2	68.67	93.93
NE.23	-	81.35	NE.5	62.69	91.78
NE.26	-	81.57	NE.15	65.19	90.85
NE.28	-	81.43	NE.19	75.48	94.42
NE.30	-	87.02	NE.29	66.13	90.97
NE.31	-	80.39	NE.32	66.75	87.33
NE.38	55.93	72.45	NE.34	75.20	93.26
NE.40	56.00	78.05	NE.36	-	87.11
NE.43	-	82.28	NE.46	-	85.48
NE.45	-	79.45	NE.48	-	87.64
NE.52	69.95	88.29	NE.50	74.07	96.13
NE.57	52.87	87.29			
NE.60	66.64	96.95			
Average	60.28	82.72	Average	69.27	90.81

7.7. Hydraulic sorting of siliciclastic deposits of the Ashin Formation

Hydraulic sorting of degraded grains plays a significant role on the chemical composition of sediments (Zaid and Al-Gahtani 2015). Chemical variability is calculated by hydraulic sorting based on Index of Compositional Variability (ICV) (Cox et al. 1995). This index is obtained from the following equation (3) which highlights Al content in relation with other major elements contents:

$$[(Fe_2O_3+K_2O+Na_2O+CaO+MgO+MnO+TiO_2)/Al_2O_3] \quad \text{(Equation 3)}$$

The rock-forming minerals such as plagioclase, K-feldspars, amphibole, and pyroxene show ICV values greater than 0.84, and presence of alteration minerals such as kaolinite, illite, and muscovite show index values lower than 0.84. (Cullers 2000; Cox et al. 1995; Moosavirad et al. 2011). The average amount of ICV in sandstone samples of the Ashin Formation is 2.18, indicating higher amounts of rock-forming minerals in these sandstones. Similarly, the average value of SiO_2 / Al_2O_3 (0.57) mentioned above indicates that these sandstone seems to have an immature chemical composition (Ahmad and Chandra 2013). The result confirms that the studied sandstone of the Ashin

Formation originated from recycled orogenic source or from severe weathering of intermediate-to felsic rocks. The average ICV value in the shale samples of the Ashin Formation is 1.36. Based on the results, these shales are immature and were deposited under an active tectonic setting (van de Kamp and Leake 1985).

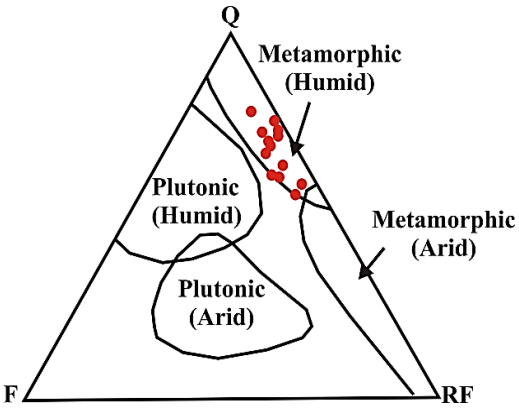

Fig 20. QFRf triangular diagram of Sutner et al. (1981) for sandstone samples of the Ashin Formation (solid red circle), Q: quartz, F: feldspar, and RF: rock fragments.

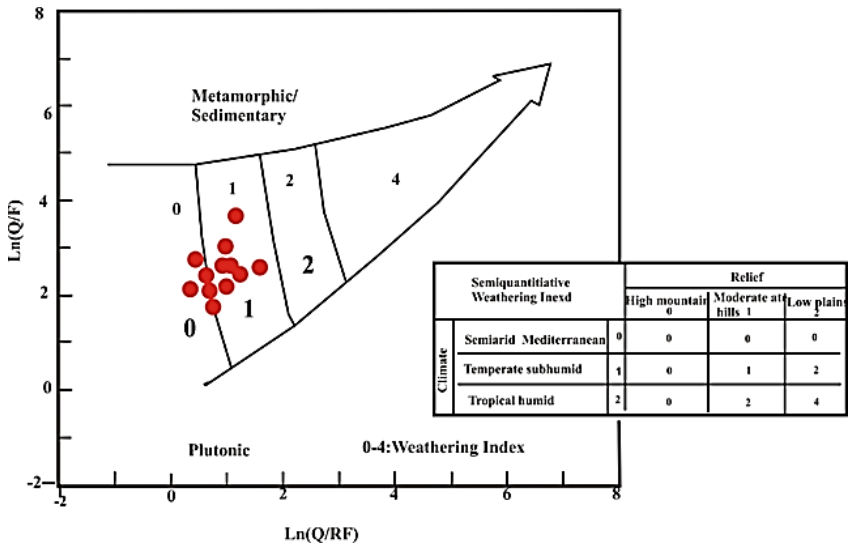

Fig 21. Logarithmic-relative diagram of Weltje et al. (1998) for sandstone samples of the Ashin Formation (solid red circles).

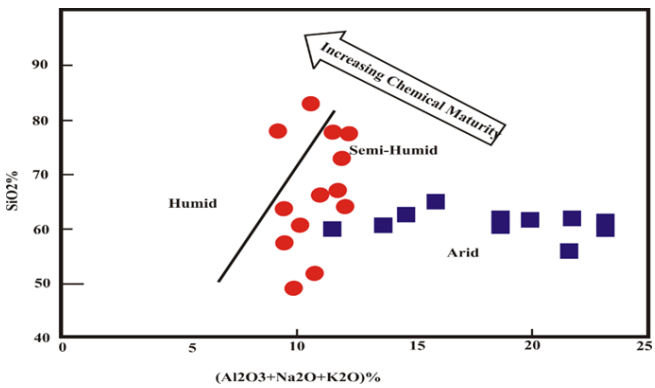

Fig 22. Long-term climate diagram of Suttner and Dutta (1986), plotting SiO_2 percentage versus total percentage of (Al_2O_3 + K_2O + Na_2O) for shale and sandstone samples of the Ashin Formation (solid red circle = sandstone samples, solid blue square = shale samples).

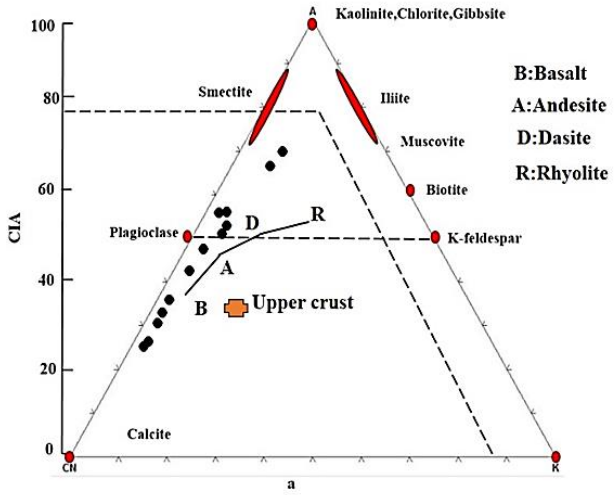

Fig 23. A-CN-K and CIA plots (after Nesbitt and Young, 1982, Nesbitt et al., 1996) for sandstones of the Ashin Formation

8. Conclusion

The Ashin Formation in the studied section overlies the Baqoroq Formation with an erosional uncomformity/contact and underlies late Cretaceous deposits with a tectonic contact. Clastic deposits of the Ashin Formation are mainly composed of sandstone and shale. The sedimentary facies associations identified in the Ashin Formation include sandstone, shale and limestone facies. The sandstone facies association consists of three petrofacies including litharenites, calclithite and graywacke, named as chert-arenite and lithicarenite due to the abundance of chert fragments. Depending on the amount of calcareous vs. siliciclastic grains, the siltstone facies includes classical siltstone, limy siltstone, and sandy siltstones. The only limestone facies is comprised by limy mudstone. The sedimentary structures observed in these deposits include parallel and cross lamination, ripple and convolute lamination. Observed trace fossils include Paleodictyon, Lorenzinia, Megagrapton and Protopaleodictyon, belonging to the Nereites ichnofacies. The study of sedimentary structures, trace fossils, lateral and vertical relations between facies and microfacies and their comparison with the Bouma sequence indicates that the Ashin Formation was probably deposited by turbidity currents in a deep-marine environment, within a submarine fan. limestone facies of the Ashin Formation include limy mudstones deposited at the upper more proximal parts of the distal submarine fan. siliciclastic facies include sandstone and shale deposited in the middle and outer parts of the distal submarine fan towards the abyssal plain. Data obtained from the geochemical analysis of major elements classify the sandstones of the Ashin formation as litharenites and sub-litharenites, with a limited number of Fe-sands also present validating petrographic studies. Comparing major elements in the studied shale and sandstone with the mean composition of the upper continental crust indicates CaO enrichment and MgO depletion in sandstones and MnO and P2O5 depletion in both shale and sandstone samples. The results of modal and geochemical analysis indicate a recycled orogenic provenance and a tectonic setting within an active continental margin /arc. Plotting of the Al_2O_3 / TiO_2 and K2O / Al2O3 ratios for shale samples of the Ashin Formation indicate a felsic intermediate to granite source rock composition for these sediments. Weathering of the source area was probably moderate in a semi-arid to semi-humid climate. In addition, CIA and CIV index analysis confirms previous results, indicating that the studied rocks are immature in chemical composition and derived from moderate weathering of intermediate-granitic source rocks. Geochemical analysis also classifieds shale samples from the Ashin Formation as immature sediments deposited in an active tectonic setting.

References

Ahmad I. Chandra R (2013) Geochemistry of loess-paleosol sediments of Kashmir Valley, India: provenance and weathering. *Journal of Asian Earth Science* 66:73–89.

Akarish AIM, El-Gohary AM (2008) Petrography and geochemistry of lower Paleozoic sandstones, East Sinai, Egypt: implications for provenance and tectonic setting. *Journal of African Earth Sciences* 52:43–54.

Alavi M, Vaziri H, Seyed-Emami K, Lasemi Y(1997) The Triassic and associated rocks of the Nakhlak and Aghdarband areas in central and northeastern Iran as remnants of the southern Turanian active continental margine. Geological Society of America, *Bulletin* 109: 1563-1575.

Ali SA, Sleabi RS, Talabani MJ, Jones BG (2017) Provenance of the Walash-Naopurdan back-arc–arc clastic sequences in the Iraqi Zagros Suture Zone. *Journal of African Earth Sciences* 125: 73-87.

Alvarez NO, Roser BP (2007) Geochemistry of black shales from the Lower Cretaceous Paja Formation, Eastern Cordillera, Colombia: source weathering, provenance and tectonic setting. *Journal of South American Earth Sciences* 23:271–289.

Amireh BS (1991) Mineral composition of the Cambrian-Cretaceous Nubian series of Jordan: provenance, tectonic setting and climatological implication. *Sediment Geol* 71: 99–119.

Armstrong-Altrin JS, Lee Y, Verma S, Ramasamy S (2004) Geochemistry of sandstones from the Upper Miocene Kudanul Formation, southern India: Implications for provenance, weathering and tectonic setting. *Journal of Sedimentary Research* 74: 167–179.

Armstrong-Altrin JS, Nagarajan R, Balaram V, Natalhy-Pineda O (2015) Petrography and geochemistry of sands from the Chachalacas and Veracruz beach areas, Western Gulf of Mexico, Mexico: constraints on provenance and tectonic setting. *Journal of South American Earth Sciences* 64, 199–216.

Azizi SHH (2018) Depositional conditions, diagenesis and provenance of sedimentary rocks of the "Nakhlak Group" northeast of Naein area, Central Iran, Ph.D.Thesis Sedimentology and sedimentary petrology, Hormozgan university, 306p.

Azizi SHH, Rezaee P (2014) Lithostratigraphy and Lithofacies of the Siliciclastic Bāqoroq Formation (Middle Triassic), Nakhlak Area, Central Iran. In STRATI 2013 (pp. 463-468). Springer, Cham.

Azizi SHH, Rezaee P, Jafarzadeh M, Meinhold G, Harami SRM , Masoodi M (2018a) Evidence from detrital chrome spinel chemistry for a Paleo-Tethyan intra-oceanic island-arc provenance recorded in Triassic sandstones of the Nakhlak Group, Central Iran. *Journal of African Earth Sciences* 143: 242-252.

Azizi SHH, Rezaee P, Jafarzadeh M, Meinhold G, Harami SRM, Masoodi M (2018b) Early Mesozoic sedimentary–tectonic evolution of the Central-East Iranian Microcontinent: Evidence from a provenance study of the Nakhlak Group. *Geochemistry* 78(3): 340-355.

Balini M, Nicora A, Berra F, Garzanti E, Levera M, Mattei M, Muttoni G, Zanchi A, Bollati I, Larghi C, Zanchetta S, Salamati R, Mossavvari F (2009) The Triassic stratigraphic succession of Nakhlak (Central Iran), a record from an active margin. *Geological Society, London, Special Publications* 312: 287-321.

Bhatia MR (1983) Plate tectonics and geochemical composition of sandstones. *Journal of Geology* 91: 611–627.

Bhatia MR, Crook KW (1986) Trace element characteristics of graywackes and tectonic setting discrimination of sedimentary basins. *Contributions to mineralogy and petrology* 92:181–93.

Blatt H (1985) Provenance studies and mudrocks. Sedimentary Petrology, 55: 69–75.

Bouma AH (1962) Sedimentology of some Flysch deposits: A graphic approach to facies interpretation. Elsevier, 168p.

Brooks HL, Hodgson DM, Brunt RL, Peakall J, Hofstra M, Flint SS (2018) Deep-water channel-lobe transition zone dynamics: Processes and depositional architecture, an example from the Karoo Basin, South Africa. *GSA Bulletin* 130(9-10): 1723-1746.

Catuneanu O (2006) Principles of Sequence Stratigraphy, Elsevier Science, 398pcentral Iran, and ist bearing for the reconstruction of the history of the Eurasian margin. In: South Caspian to Central Iran Basins (M.-F. Brunet, M. Wilmsen and J. Granath, eds), Geol. Soc. Lond. Spec. Publ., 312, 261–286. classified by grain size and feeder system. *AAPG Bull* 78: 792–822.

Coe AL (2003) The sedimentary record of sea-level change. Black Well, open, 452p.

Condie KC (1993) Chemical composition and evolution of the upper continental crust: contrasting results from surface samples and shales. *Chemical geology* 104:1–37.

Cox R, Low DR, Cullers RL (1995) The influence of sediment recycling and basement composition on evolution of mudrock chemistry in the southwestern United States. *Geochimica et Cosmochimica Acta* 59: 2919–2940.

Crook KAW (1974) Lithogenesis and geotectonics: the significance of compositional variations in flysch arenites (graywackes). In: DottJr. Jr., R.H., Shaver, R.H. (Eds.), Modern and Ancient Geosynclinal Sedimentation. *SEPM Special Publications* 19: 304–310.

Cullers RL (1995) The controls on the major and trace element evolution of shales, siltstone and sandstone of Ordovician to Tertiary age in the Wet Mountains region, Colorado, USA. *Chemical Geology* 123 (1-4): 107-131.

Cullers RL (2000) The geochemistry of shales, siltstones and sandstones of Pennsylvanian-Permian age, Colorado, USA: Implications for provenance and metamorphic studies. *Lithos* 51:181–203.

Cullers, RL (1994) The chemical signature of source rock in size fractions of Holocene stream sediment derived from metamorphic rock in the Wet Mountains region, USA. *Chemical Geology* 113: 327-343.

Das B K, AL-Mikhalafi AS, Kaur P (2006) Geochemistry of Mansar Lake sediments, Jammu, India: Implication for source-area weathering, provenance, and tectonic setting. *Journal of Asian Earth Science* 26:649-668.

Davoudzadeh M, Seyed-Emami K (1972) Stratigraphy of the Triassic Nakhlak Group. Anarak Region, Central lran, Geol. Surv. *Iran Rep* 28: 1- 28.

Dey S, Rai AK, Chaki A (2009) Palaeoweathering, composition and tectonics of provenance of the Proterozoic intracratonic Kaladgi-Badami basin, Karnataka, southern India: evidence from sandstone petrography and geochemistry. *Journal of Asian Earth Sciences* 34:703–715.

Dickinson WR, Beard LS, Brakenridge GR, Erjavec JL, Ferguson RC, Inman KF. Knepp RA, Lindberg FA, Ryberg PT (1983) Provenance of North American Phanerozoic sandstones in relation to tectonic setting. *Geological Society of American Bulletin* 94: 222–235.

Dickinson WR, Suczek C (1979) Plate tectonics and sandstone composition. *American Association of Petroleum Geologists Bulletin* 63:2164–2182.

Dunham RG (1962) Classification of carbonate rocks according to depositional texture. In W. E. Ham(ED), classification of carbonate Rocks. *american Association of petroleum Geologists Memoir* 1:108-121.

Embry AF, Klovan J E (1971) A Late Devonian reef tract on Northeastern Banks Island, NWT: *Canadian Petroleum Geology Bulletin* 19: 730-781.

Fedo CM, Nesbitt HW, Young GM (1995) Unraveling the effects of K-metasomatism in sedimentary rocks and paleosols, with implications for paleoweathering conditions and provenance. *Geology* 23:921–924.

Flugel E (2010) Microfacies of Carbonate Rocks, Analaysis, Interpretation and Application Springer-Verlag, Berlin, Heidelberg, NewYork, 976 p.

Folk RL (1980) Petrology of Sedimentary Rocks. Hemphill Publishing Co., Austin, Texas, 182p.

Gabo JAS, Dimalanta CB, Asio MGS, Queaño KL Yumul JrGP, Imai A (2009) Geology and geochemistry of the clastic sequences from Northwestern Panay (Philippines): Implications for provenance and geotectonic setting. *Tectonophysics* 479(1-2): 111-119.

Garcia D, Ravenne C, Maréchal B, Moutte J (2004) Geochemical variability induced by entrainment sorting: quantified signals for provenance analysis. *Sedimentary Geology* 171:113-128.

Ghorbani M (2019) Lithostratigraphy of Iran, Springer, 296p.

Ghosh S, Sarkar S (2010) Gheochemistry of Permo-Triassic mudstone of the Satpura Gondwana basin, central India: Clues for provenance. *Chemical Geology* 277: 78-100.

Harnois L (1988) The CIW index: a new chemical index of weathering. *Sedimentary Geology* 55:319–322.

Hashemi Azizi S, Rezaee P, Moussavi Harami S, Jafarzadeh M, Masoodi M (2017) provenance of siliciclastic Baqoroq Formation, Central Iran, based on petrography and geochemistry: *Implication for the evolution of active margin of south Eurasia. Journal of Stratigraphy and Sedimentology Researches* 33(2): 18-40.

Hayashi K, Fujisawa H, Holland HD, Ohmoto H (1997) Geochemistry of ~1.9 Ga sedimentary rocks from northeastern Labrador, *Canada. Geochimica et Cosmochimica Acta* 61:4115–4137.

Herron MM (1988) Geochemical classification of terrigenous sands and shales from core or log data. *Journal of Sedimentary Petrology* 58: 820-829.

Hessler AM, Lowe D.M (2006) Weathering and sediment generation in the Archean: An integrated study of the evolution of siliciclastic sedimentary rocks of the 3.2 Ga Moodies Group, Barberton Greenstone Belt, South Africa. *Precambrian Research* 151: 185-210.

Ingersoll RV, Bullard T, Ford R, Grimm J, Pickle J, Sares S (1984) The effect of grain size on detrital modes: *a test of the Gazzi Dickinson point-counting method. Journal of Sedimentary Petrology* 54: 103–116.

Jafarzadeh M, Hosseini-Barzi M (2008) Petrography and geochemistry of Ahwaz sandstone member of Asmari Formation, Zagros, Iran: *implications on provenance and tectonic setting. Revista Mexicana de Ciencias Geologicas* 25 (2): 247–260.

Jafarzadeh M, Harami RM, Amini A, Mahboubi A, Farzaneh F (2013) Geochemical constraints on the provenance of Oligocene-Miocene siliciclastic deposits (Zivah Formation) of NW Iran: implications for the tectonic evolution of the Caucasus. *Arabian Journal of Geosciences* 7:4245-4263.

Jahn BM, Glikson AY, Peucat JJ, Hickman AH (1981) REE geochemistry and isotopic data of Archaean silisic volcanics and granitoids from the pilbara block, Western Australia: *implications for the early crustal evolution. Geochimica et Cosmochimca Acta* 45:1633–1652.

Jin Z, Li F, Cao J, Yu J (2006) Geochemistry of Daihai Lake sedimenys, Inner Mongolia, north China: Implications for provenance, sedimentary sorting and catchment weathering. *Geomorphology* 80:147-163.

Lee YI (2002) Provenance derived from the geochemistry of late Paleozoic–early Mesozoic mudrocks of the Pyeongan Supergroup, *Korea. Sedimentary Geology* 149:219– 235.

Lopez JMG, Bauluz B, Nieto CF, Oliete AY (2005) Factors controlling the trace-element distribution in fine-grained rocks: The Albian Kaolinite-rich deposits of the Oliete Basin (NE Spain). *Chemical Geology* 214: 1-19.

Manikyamba C, Kerrich R, Gonzalez-Alvarez I, Mathur M, Khanna CT (2008) Geochemistry of Paleoproterozoic black shales from the Intracontinental Cuddapah basin, India: implications for provenance, tectonic setting, and weathering intensity. *Precambrian Research* 162:424–440.

Maynard JB, Valloni R, Yu HS (1982) Composition of Modern Deep-sea Sands from Arc-related Basins. Geological Society, London, *Special Publications* 10: 551–561.

McBride EF (1985) Diagenetic processes that affect provenance determination in sandstone. In Zuffa G. G. (ed.), Provenance in Arenites. *Reidel Publishing Company* 407: 95-113.

McLennan SM (2001) Relationships between the trace element composition of sedimentary rocks and upper continental crust. Geochemistry, Geophysics, Geosystems, 2, C000109.

McLennan SM, Taylor SR, Eriksson KA (1983) Geochemistry of Archaean shales from the Pilbara

Supergroup, *Western Australia. Geochimica et Cosmochimica Acta* 47:1211–1222.

Miall A (2000) The geology of stratigraphic sequences, springer Heidelberg Mojsisovics, E., von, 1893, Faunistische Ergebnisse aus der Untersuchung der Ammoneen-faunen der Mediterranen Trias. *Abhandlungen der Geologischen Reichsanstalt* 6: 810.

Mishra M, Sen S (2010) Geological signatures of Mesoproterozoic siliciclastic rocks of the Kaimur Group of the Vindhyan Supergroup, Central India. *Chinese Journal of Geochemistry* 20:2132.

Moosavirad SM, Janardhana MR, Sethumadhav MS, Moghadam MR, Shankara M (2011) Geochemistry of lower Jurassic shales of the Shemshak Formation, Kerman Province, Central Iran: Provenance, source weathering and tectonic setting. *Chemie der Erde-Geochemistry* 71: 279–288.

Nagarajan R, Armstrong-Altrin JS, Kessler FL, Jong J (2017) Petrological and geochemical constraints on provenance, paleoweathering, and tectonic setting of clastic sediments from the Neogene Lambir and Sibuti Formations, northwest Borneo, in: Mazumder, R., (Eds.), Sediment provenance: Influence on compositional change from source to sink, *Elsevier science* 600: 123-153.

Nagarajan R, Roy PD, Jonathan MP, Lozano-Santacruz R, Kessler FL, Prasanna MV (2014.) Geochemistry of Neogene sedimentary rocks from Borneo basin, East Malaysia: paleo-weathering, provenance and tectonic setting. *Chemie der Erde- Geochemistry* 74 (1): 139-146.

Nath BN, Kunzendorf H, Pluger WL (2000) Influence of provenance, weathering and sedimentary processes on the elemental ratio of the fine-grained fraction of the bed load sediments from the Vembanad Lake and the adjoining continental shelf, southwest Coast of India. *Journal of Sedimentary Research* 70:1081–1094.

Nesbitt HW, Young GM (1989) Formation and diagenesis of weathering profiles. *Journal of Geology* 97:129 147.

Nesbitt HW, Young G M (1984) Prediction of some weathering trends of plutonic and volcanic rocks based on thermodynamic and kinetic considerations. *Geochimica et Cosmochimica Acta* 48:1523–1534.

Nesbitt HW, Young GM (1982) Early Proterozoic climates and plate motions inferred from mayor element chemistry of lutites. Nature, 299:715–717.

Nichols G (2009) Sedimentology and stratigraphy, 2nd ed. Wiley-Blackwell, 419 p.

Nikbakht, S T. Rezaee P. Moussavi-Harami R. Khanehbad M. and Ghaemi F (2019) Facies analysis, sedimentary environment and sequence stratigraphy of the Khan Formation in the Kalmard Sub-Block, Central Iran: implications for Lower Permian palaeogeography. *Neues Jahrbuch für Geologie und Paläontologie-Abhandlungen 292*(2): 129-154.

Nowrouzi Z, Moussavi-Harami R, Mahboubi A, Gharaie MHM, Ghaemi F (2013) Petrography and geochemistry of Silurian Niur sandstones, Derenjal Mountains, East Central Iran: implications for tectonic setting, provenance and weathering. *Arabian Journal of Geosciences* 7:2793–2813.

Osae S, Asiedu D K, Banoeng-Yakubo B, Koeberl C, Dampare SB (2006) Provenance and tectonic setting of Late Proterozoic Buem sandstones of southeastern Ghana: Evidence from geochemistry and detrital modes. *Journal of African Earth Sciences* 44(1): 85-96.

Paikaray S, Banerjee S, Mukherji S (2008) Geochemistry of shales from the Paleoproterozoic to NeoproterozoicVindhyan Supergroup: Implications on provenance, tectonics and paleoweathering. *Journal of Asian Earth Sciences* 32:34–48.

Pettijohn FJ, Potter PE, Siever R (1987) Sand and Sandstone, 2nd edition. Springer-Verlag, New York, 553p.

Raza M, Dayal AM, Khan A, Bhardwaj VR, Rais S (2010) Geochemistry of lower Vindhyan clastic sedimentary rocks of Northwestern Indian shield: Implications for composition and weathering history of Proterozoic continental crust. *Journal of African Earth Sciences* 39:51–61.

Reading HG, Richards M (1994) Turbidite systems in deep-water basins classified by grain-size and feeder system. *Bulletin of the American Association of Petroleum Geologists* 78: 792–822.

Rollinson HR (1993) Using Geochemical Data: Evaluation, Presentation, Interpretation. Longman Scientific and Technical, New York. 352pp.

Roser BP, Korsch RJ (1986) Determination of tectonic setting of sandstone-mudstone suites using SiO2 content and K_2O/Na_2O ratio. *Journal of Geology* 94: 635–65.

Roser BP, Korsch RJ (1988) Provenance signature of sandstone-mudstone suite determined using discriminate function analysis of major element data. *Chemical Geology* 67:119–139.

Rudnick RL, Fountain DM (1995) Nature and composition of the continental crust: a lower crustal perspective. *Reviews of geophysics* 33:267-309.

Ruttner AW (1991) Geology of the Aghdarband Area (Kopet Dagh. NE-lran). Abh. Geol. 38: 7–79.

Ruttner AW (1993) Southern borderland of Triassic Laurasia in north-east Iran. *Geologische Rundschau* 82: 110–120.

Saxena A, Pandit MK (2012) Geochemistry of Hindoli Group metasediments, SE Aravalli craton NW India: implications for palaeoweathering and provenance. *Journal of the Geological Society of India* 79:267–278.

Schieber J (1992) A combined petrographical-geochemical provenance study of the Newland formation, Mid-Proterozoic of Montana. *Geological Magazine* 129:223–237.

Schwab FL (1975) Framework mineralogy and chemical composition of continental margin type sandstone. *Geology* 3:487–490.

Seilacher A (2007) Trace fossil analysis. Springer Science & Business Media.

Seyed-Emami, K 2003. Triassic of Iran. *Facies* 48: 91–106.

Spalletti LA, QueraltI, Matheos SD, Colombo F, Maggi J (2008) Sedimentary petrology and geochemistry of siliciclastic rocks from the upper Jurassic Tordillo Formation (Neuquén Basin, western Argentina): implications for provenance and tectonic setting. *Journal of South American Earth Sciences* 25:440–463.

Stow DAV (2005) Sedimentary Rocks in the Field. A Colour Guide. 320 pp.

Suttner LJ, Dutta PK (1986) Alluvial sandstone composition and palaeoclimate: framework mineralogy. *Journal of Sedimentary Petrology* 56:329–345.

Suttner LJ, Basu A, Mack GH (1981) Climate and the origin of quartz arenites. *Journal of Sedimentary Research* 51:235–246.

Taylor SR. McLennan S (1985) The Continental Crust: Its Composition and Evolution, Blackwell, Oxford, 312pp.

Tudor EP (2014) Facies variability in deep water channel-to-lobe transition zone: Jurassic Los Molles Formation, Neuquen Basin, Argentina (Doctoral dissertation).

van de Kamp PC, Leake BE (1985) Petrography and geochemistry of feldspathic and mafic sediments of the northeastern Pacific margin. *Earth and Environmental Science Transactions of the Royal Society of Edinburgh* 76:411–449.

Van der Merwe WC, Hodgson DM, Brunt RL Flint SS (2014) Depositional architecture of sand-attached and sand-detached channel-lobe transition zones on an exhumed stepped slope mapped over a 2500 km2 area. *Geosphere*, 10(6): 1076-1093.

Vaziri SH (2001) The Triassic Nakhlak Group, an exotic succession in Central Iran. In: Akinci, Ö.T., Görmüş, M., Kuşçu, M., Karagüzel, R., Bozcu, M. (Eds.), Proceedings of the 4th International Symposium on Eastern Mediterranean Geology, Isparta, *Turkey* 53–68.

Vaziri SH (2011) Sedimentary structures and depositional environment of the Ashin Formation in Nakhlak area, Central Iran. *Iranian Journal of Earth Sciences* 3: 253-263.

Verma SP, Armstrong-Altrin JS (2013) New multi-dimensional diagrams for tectonic discrimination of siliciclastic sediments and their application to Precambrian basins. *Chemical Geology* 355: 117–133.

Von Eynatten HV (2003) Petrography and chemistry of sandstones from the Swiss Molasse Basin: an archive of the Oligocene to Miocene evolution of the Central Alps. *Sedimentology* 50: 703–724.

Weltje GJ, Meijer XD, De Boer PL(1998) Stratigraphic inversion of siliciclastic basin fills: a note on the distinction between supply signals resulting from tectonic and climatic forcing. *Basin Research* 10:129–153.

Wilson JL (1975) Carbonate facies in geologic history. Springer, Berlin, 471p.

Wronkiewicz DJ, Condie KC (1987) Geochemistry of Archean shales from the Witwatersrand Supergroup, South Africa: source-area weathering and provenance. *Geochimica et Cosmochimica Acta* 51:2401–2416.

Zaid SM, Al-Gahtani F (2015) Provenance, diagenesis, tectonic setting, and geochemistry of Hawkesbury Sandstone (Middle Triassic), southern Sydney Basin, Australia. Turkish Journal of Earth Sciences, 24:72-98.

Zhang KL (2004) Secular geochemical variations of the Lower Cretaceous siliciclastic from central Tibet (China) indicate a tectonic transition from continental collision to back-arc rifting. *Earth and Planetary Science Letters* 229:73–89.

Zimmermann U Bahlburg H (2003) Provenance analysis and tectonic setting of the Ordovician clastic deposits in the southern Puna Basin, NW Argentina. *Sedimentology* 50: 1079–1104.